

Review:

Dispersion-engineered wideband low-profile metasurface antennas*

Wei E. I. LIU^{‡1}, Zhi Ning CHEN¹, Xianming QING²

¹Department of Electrical and Computer Engineering, National University of Singapore, Singapore 117583, Singapore

²Institute for Infocomm Research, Singapore 138632, Singapore

E-mail: jociou.ustc@gmail.com; eleczn@nus.edu.sg; qingxm@i2r.a-star.edu.sg

Received Sept. 4, 2019; Revision accepted Dec. 12, 2019; Crosschecked Jan. 3, 2020

Abstract: A metasurface (MTS) can be characterized in terms of dispersion properties of guided waves and surface waves. By engineering the rich dispersion relations, setting particular boundary conditions, and selecting proper excitation schemes, multiple adjacent resonance modes can be excited to realize the wideband operation of low-profile MTS antennas. We introduce the operating principles of typical dispersion-engineered MTS antennas, and review the recent progress in dispersion-engineered MTS antenna technology. The miniaturization, circular polarization, beam-scanning, and other functionalities of MTS antennas are discussed. The recent development of MTS antennas has not only provided promising solutions to the wideband and low-profile antenna design but also proven great potential of MTS in developing innovative antenna technologies.

Key words: Metasurface antenna; Dispersion engineering; Composite right/left-handed (CRLH); Guided wave; Surface wave; Wideband; Low profile

<https://doi.org/10.1631/FITEE.1900473>

CLC number: TN82

1 Introduction

Due to the exhibited exotic and useful electromagnetic properties, metamaterials have attracted great interest (Smith et al., 2000; Shelby et al., 2001; Caloz and Itoh, 2005; Eleftheriades and Balmain, 2005). Metasurface (MTS) is a surface version of metamaterials, consisting of a two-dimensional (2D) array of electrical small cells to control the electromagnetic waves/fields to achieve unique properties. Due to the easy fabrication of such a 2D structure, MTSs have been extensively explored in various

applications in recent years (Holloway et al., 2012; Chen HT et al., 2016; Glybovski et al., 2016; Li AB et al., 2018). In particular, MTSs have been used to improve the performance or achieve additional functionalities of antennas by flexibly controlling reflection and transmission properties of incident electromagnetic waves. For instance, the phase gradient MTSs have been applied to the flat focusing lens design to increase the antenna gain (Li HP et al., 2015; Erfani et al., 2016). The planar MTS lens antenna system has been applied in the spatial beamforming and multibeam design for the 5th generation mobile networks (5G) massive multiple-input multiple-output (MIMO) applications at 28-GHz band (Jiang et al., 2017).

MTS can be engineered to realize unusual dispersion properties of guided/surface waves, including composite right/left-handed (CRLH) guided wave dispersion, right-handed (RH) guided wave dispersion with a zero-propagation constant at a specific

[‡] Corresponding author

* Project partially supported by the Agency for Science, Technology and Research (A*STAR), Singapore, through its Industry Alignment Fund—Pre-Positioning Programme (IAF-PP) (No. A1897a0040)

 ORCID: Wei E. I. LIU, <https://orcid.org/0000-0002-3083-0166>; Zhi Ning CHEN, <https://orcid.org/0000-0002-3617-6468>; Xianming QING, <https://orcid.org/0000-0002-8737-3234>

© Zhejiang University and Springer-Verlag GmbH Germany, part of Springer Nature 2020

non-zero frequency, and controllable surface wave (SW) dispersion.

Since the first demonstration of the wideband thin aperture-coupled CRLH MTS antenna (Liu et al., 2014a, 2014b, 2014c, 2015b), the dispersion-engineered MTSs have been intensively studied for various wideband low-profile antenna designs. By slotting a conventional microstrip patch and selecting an aperture coupling structure, a capacitively loaded MTS antenna with thickness of $0.06\lambda_0$ (λ_0 is the free-space wavelength at the center operating frequency) can achieve a bandwidth of 30% in terms of both impedance matching and consistent radiation performances. In this design, the dispersion properties of a conventional patch antenna can be engineered by introducing a capacitive slot load.

We review the recent progress in the development of dispersion-engineered wideband low-profile MTS antennas. The operating mechanism and design of three types of wideband dispersion-engineered MTS antennas, i.e., CRLH MTS antennas, RH MTS antennas, and surface wave resonant (SWR) MTS antennas, are introduced. The miniaturization techniques of wideband dispersion-engineered MTS antennas are discussed. A variety of multifunction wideband MTS antennas, including the circularly polarized (CP), beam-steering, low radar cross-section (RCS), filtering, shared-aperture dual band, and reconfigurable antennas, are reviewed.

2 Dispersion-engineered MTS antennas

The transverse dispersion properties of MTS are explored for the wideband low-profile MTS antennas with consistent radiation performance. Three types of dispersion-engineered MTS antennas are reviewed to present the operating mechanism of MTS antennas.

2.1 CRLH MTS antennas

A typical CRLH MTS is composed of a 2D array of mushroom-like unit cells (Fig. 1). The simulation model and equivalent circuit of the mushroom-like MTS unit cells are presented in Fig. 1a. Unbalanced CRLH dispersion of guided waves in the CRLH MTS is shown in Fig. 1b, owing to the series capacitor C_L created by gaps between the upper patches and the shunt inductor L_L created by the shorting vias connecting the upper patches and the bottom ground

plane. The series inductor L_R and shunt capacitor C_R contribute to the RH branch, while the series capacitor C_L and the shunt inductor L_L form an LH dual counterpart. Depending on specific boundary conditions, only one particular zeroth-order resonance (ZOR) is excited. For the open-ended MTS resonator, the shunt ZOR occurs at the frequency of $f_{sh} = 1/\left(2\pi\sqrt{L_L C_R}\right)$, while for the short-ended one, the series ZOR happens at the frequency of $f_{se} = 1/\left(2\pi\sqrt{L_R C_L}\right)$.

Compared with conventional microstrip patch, the CRLH MTS can generate multiple resonances including the positive-, zeroth-, and negative-order resonances. Therefore, the dispersion-engineered CRLH MTS provides great freedom and potential in the wideband low-profile antenna design.

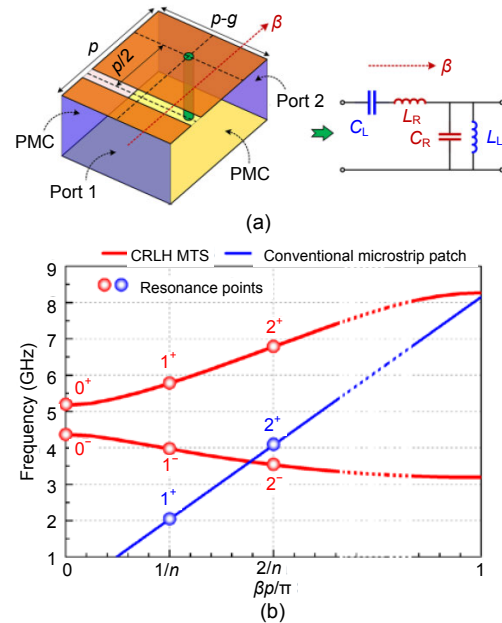


Fig. 1 CRLH MTS unit cell: (a) simulation model and equivalent circuit; (b) CRLH dispersion diagram

References to color refer to the online version of this figure

2.1.1 Open-ended CRLH MTS antennas

By applying the aperture coupling scheme to an open-ended CRLH MTS, a wideband low-profile antenna solution could be successfully developed by exciting two adjacent positive-order resonances (Liu et al., 2014a), as shown in Fig. 2. The fabricated MTS antenna composing an array of square mushroom-like unit cells, fed by a microstrip line through a coupling aperture cut on the common ground plane, is shown in

Fig. 2a. With the dispersion-engineered guided waves (Fig. 2b), the aperture-coupled open-ended CRLH MTS generates a TM_{10} mode and an antiphase TM_{20} mode at the first- and second-order positive resonances, respectively. The electric field distributions of these two modes are illustrated in Fig. 2c. Under the antiphase TM_{20} mode, the directions of electric fields at the opposite sides of the center aperture coupling region are antiparallel. Thus, TM_{10} mode and antiphase TM_{20} mode both produce the boresight radiation, and their resonance frequency ratios can be controlled by engineering the dispersion of the guided wave to achieve the wideband operation. As shown in Fig. 2d, the measured -10 -dB impedance bandwidth is in the range of 4.77–6.16 GHz (25.4%) with the realized gain ranging from 8.7 to 10.8 dBi, while the thickness of the MTS is $0.06\lambda_0$ (λ_0 represents the free-space wavelength at the center operating frequency of 5.47 GHz). To suppress the relatively high backlobe levels, a stripline-fed aperture coupling

structure can be used, as presented in Liu et al. (2014b).

Furthermore, the open-ended CRLH MTS antenna technology can be employed to realize a wideband high-gain array in the low temperature co-fired ceramic (LTCC) at the 60-GHz band (Fig. 3a) (Liu et al., 2014c). By replacing the microstrip line fed with a substrate integrated waveguide (SIW) feeding network, the back lobe levels of the array antenna can be greatly reduced. The weak mutual coupling between the MTS antenna elements is revealed through the comparison with conventional patch counterparts. As shown in Figs. 3b and 3c, an MTS array with a low profile of $0.04\lambda_0$ (λ_0 is the free-space wavelength at the center operating frequency of 61 GHz) and a substrate dielectric constant of 5.9 can achieve a measured bandwidth in the range of 56.3–65.7 GHz (15%) for $|S_{11}| < -10$ dB, a realized gain ranging from 21.2 to 24.2 dBi, and a front-to-back ratio (FBR) of larger than 30 dB.

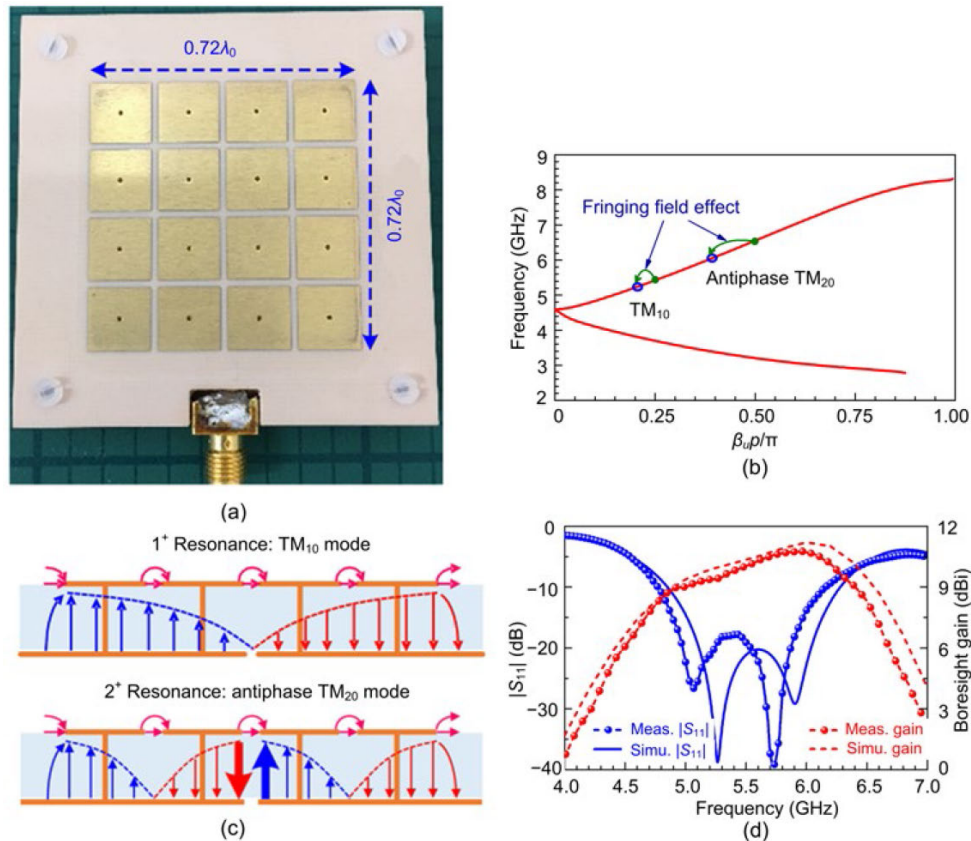


Fig. 2 Open-ended CRLH MTS antenna: (a) a photograph of the prototype; (b) dispersion diagram of the CRLH MTS unit; (c) electric field distributions with a TM_{10} mode and an antiphase TM_{20} mode; (d) measured and simulated $|S_{11}|$ and realized boresight gain

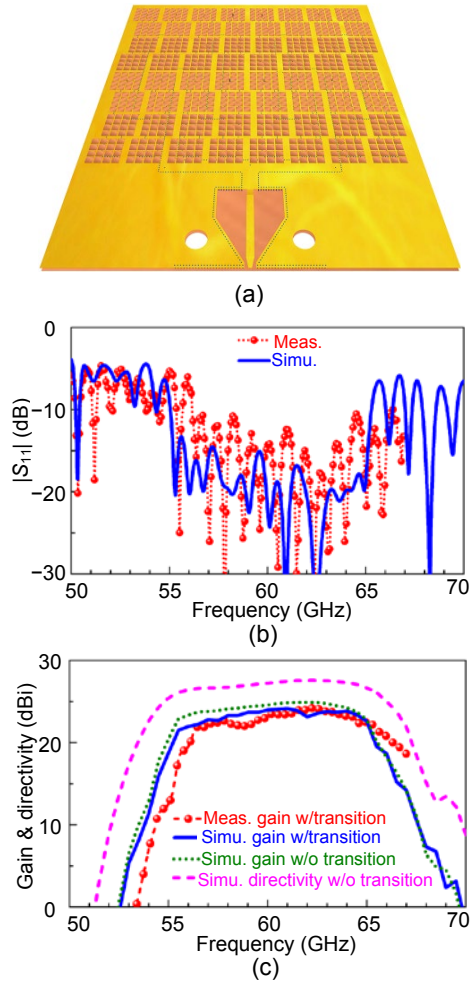


Fig. 3 60-GHz LTCC SIW-fed CRLH MTS array antenna: (a) antenna structure; (b) measured and simulated $|S_{11}|$; (c) realized boresight gain

References to color refer to the online version of this figure

2.1.2 Short-ended CRLH MTS antennas

Fig. 4a shows the aperture-coupled short-ended CRLH MTS antenna, wherein two rows of shorting vias are introduced to form a short-ended boundary of the MTS (Liu et al., 2017d). Fig. 4b depicts the engineered dispersion of the composed mushroom-like unit cell. Once the open-ended boundary condition is altered to the short-ended case, the operating modes of the CRLH MTS antenna change; that is to say, the series ZOR mode is excited, and then an antiphase TM_{10} mode is enforced at the first-order positive resonance (Fig. 4c). Both modes generate an in-phase mission from the radiating gaps between the upper patches of the MTS. As illustrated in Fig. 4d, the

short-ended CRLH MTS antenna has a -10 -dB impedance bandwidth in the range of 4.74–6.36 GHz (29%) at a low profile of $0.06\lambda_0$ (λ_0 is the free-space wavelength at the center operating frequency of 5.5 GHz). Since the series ZOR mode and antiphase TM_{10} mode move to the lower band of the RH dispersion branch, a short-ended CRLH MTS has a smaller aperture size of $0.63\lambda_0 \times 0.61\lambda_0$ compared with an open-ended counterpart, thus resulting in a relatively lower gain in the range of 7.5–9.4 dBi.

2.2 RH MTS antennas

As the operating modes of all the aforementioned CRLH MTS antennas are located at the RH dispersion branch, the LH dispersion branch is not necessary. Therefore, the shunt shorting vias can be removed to obtain the RH dispersion with a zero-propagation constant at a specific non-zero frequency, i.e., the series ZOR frequency. Fig. 5a depicts the dispersion extraction model and the equivalent circuit model of the via-less RH MTS. The pure RH dispersion of the MTS is controllable through the effective series capacitor (C_L) brought about by the gaps between the upper patches. The photograph of an aperture-coupled open-ended RH MTS antenna and the RH dispersion of its via-less unit cell are shown in Figs. 5b and 5c, respectively (Liu et al., 2015a). As illustrated in Fig. 5d, TM_{10} mode and antiphase TM_{20} mode can be retained in an RH MTS antenna. Fig. 5e shows that the RH MTS of $0.7\lambda_0 \times 0.7\lambda_0 \times 0.06\lambda_0$ (λ_0 is the free-space wavelength at the center operating frequency of 5.4 GHz) can provide a simulated -10 -dB impedance bandwidth of 29% with the realized gain ranging from 7.4 to 10.6 dBi.

The open-ended via-less RH MTS antenna stands out as a low-cost solution while achieving the performance similar to that of the CRLH MTS antenna with vias, especially in the large-scale array applications where a huge number of vias can be exempt. In addition, it is believed that the short-ended via-less RH MTS is applicable to the low-profile wideband antenna design by simultaneously exciting the series ZOR mode and the antiphase TM_{10} mode.

Since the successful demonstration of the wideband low-profile RH MTS antenna (Liu et al., 2015a), various RH MTS antennas with different feeding methods are developed. For instance, a high mode SIW cavity can be employed to realize a

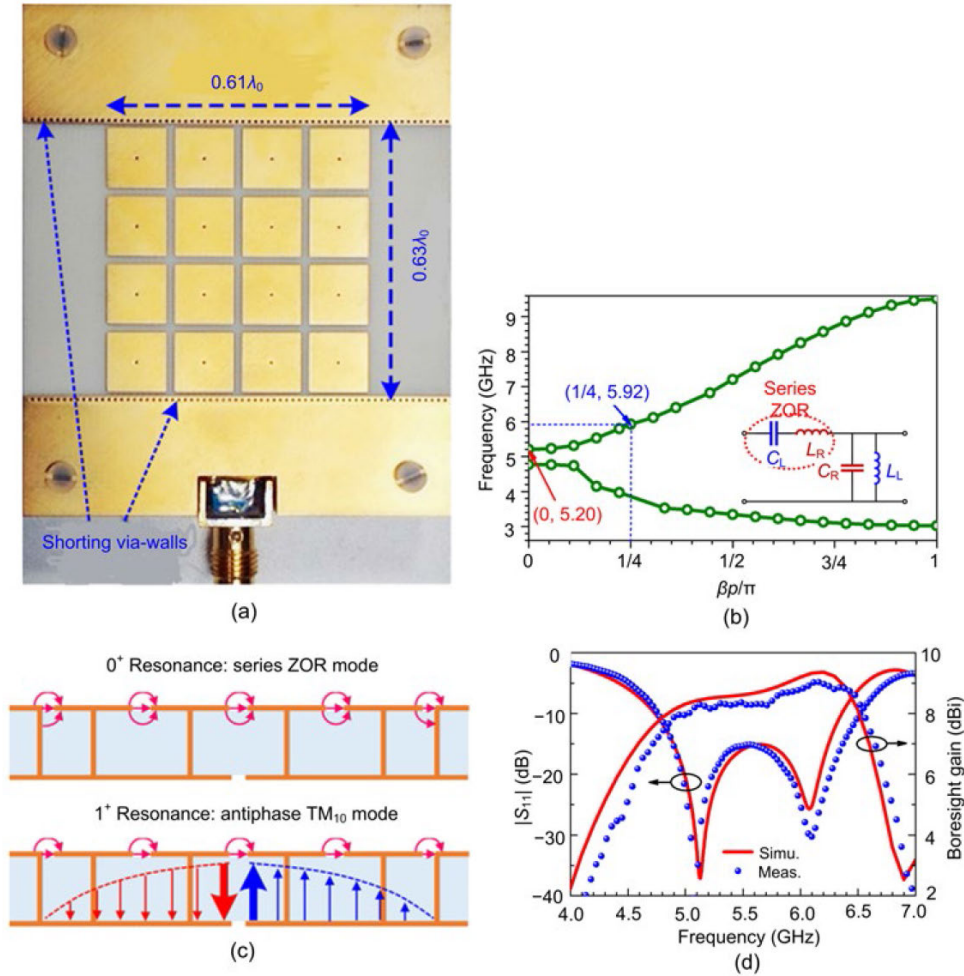


Fig. 4 Short-ended CRLH MTS antenna: (a) a photograph of the prototype; (b) dispersion diagram of the CRLH MTS unit; (c) electric field distributions with the series ZOR mode and the antiphase TM_{10} mode; (d) measured and simulated $|S_{11}|$ and realized boresight gain

compact high-gain MTS antenna (Yang et al., 2018). A single-layer quasi-periodic MTS antenna with a slot-to-CPW transition can achieve a bandwidth of 35% with a low profile of $0.052\lambda_0$ (Sun et al., 2019). A single-layer CPW-fed stair-aperture-coupled MTS antenna with a profile of $0.09\lambda_0$ extends the bandwidth up to 67% with the peak gain of 9.2 dBi (Wang et al., 2019). An aperture-coupled non-periodic square-ring MTS antenna can achieve a -10 -dB impedance bandwidth of 54% and a 2-dB gain bandwidth of 32% at a profile of $0.06\lambda_0$ (Chen et al., 2019).

2.3 SWR MTS antennas

Usually, the presence of surface waves would deteriorate the radiation performance of antennas. The high impedance surface (HIS) can be characterized in terms of the zero reflection phase for low-

profile antenna design as well as the forbidden frequency band for suppressing surface waves (Sievenpiper et al., 1999; Yang and Rahmat-Samii, 2003). However, the surface waves propagating in a finite HIS can be used to create an additional resonance for improving the performance of antennas. The transverse electric (TE) surface wave resonance is excited by a horizontal dipole antenna over a finite HIS (Costa et al., 2011). The finite HIS-dipole antenna with a profile of $0.04\lambda_0$ achieves a bandwidth of 19% with stable broadside radiation.

To further improve the gain and widen the bandwidth of the antenna, a suspended MTS-based dipole antenna is proposed by engineering the dispersion properties of both the transverse magnetic (TM) wave and TE surface wave (Syed Nasser et al., 2018). Fig. 6a shows the structure of an SWR MTS

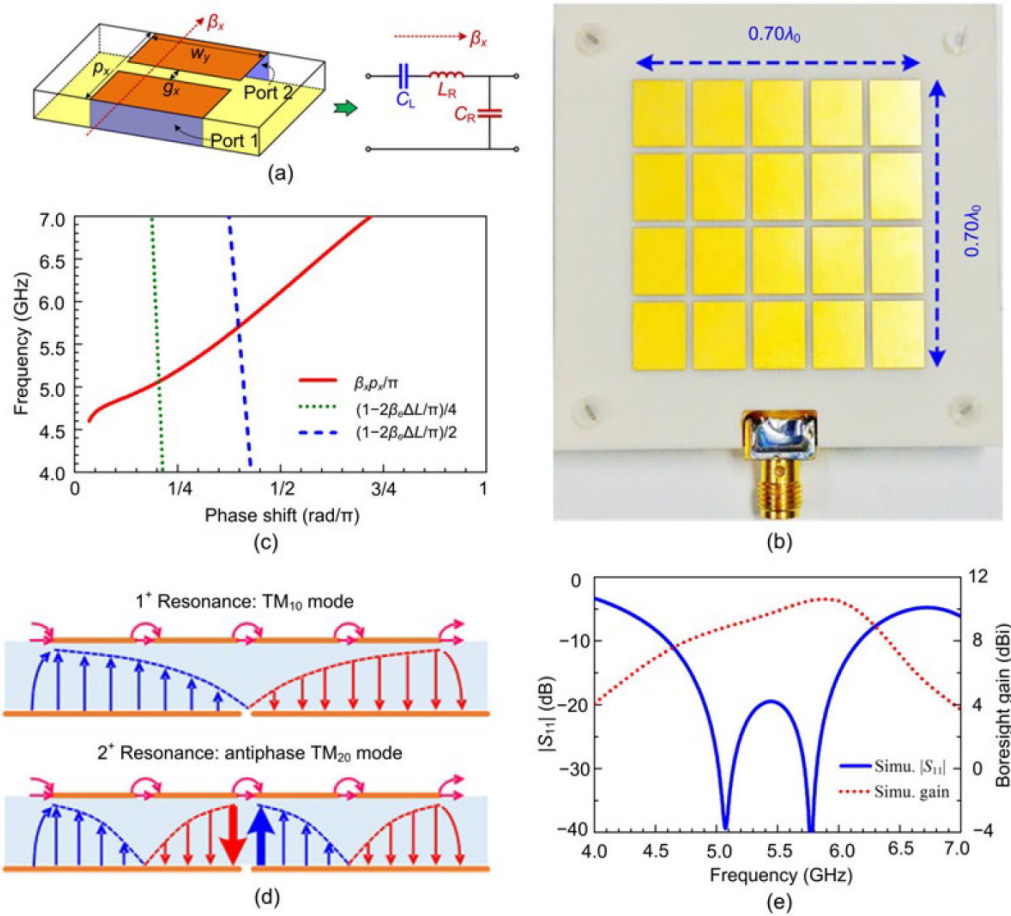


Fig. 5 Open-ended RH MTS antenna: (a) simulation model and equivalent circuit of the RH MTS unit; (b) a photograph of the prototype; (c) dispersion diagram of the RH MTS unit; (d) electric field distributions with TM₁₀ mode and anti-phase TM₂₀ mode; (e) simulated $|S_{11}|$ and realized boresight gain

antenna. The MTS is separated from the ground plane by an air gap and positioned right beneath a horizontally oriented dipole. The surface wave dispersion of the suspended MTS unit cell is shown in Fig. 6b. The dispersion of the TM SW curve could be bent to that of the light line by introducing the air gap, while the dispersion of the TE SW depends highly on the effective capacitance of the MTS layer (Luukkonen et al., 2008). A small propagation constant of the TM SW that enables a large MTS aperture along the dipole direction can be adopted for gain enhancement, while decreasing the number of MTS cells along the lateral direction of the dipole would shift the TE SW frequency upwards for widening the bandwidth and maintaining the broadside radiation patterns in the H-plane. With a low profile of $0.07\lambda_0$, a suspended MTS antenna retains the -10 -dB impedance bandwidth in the range of 4.15–5.85 GHz or 33.6%,

achieving the realized gain ranging from 8.5 to 11.5 dBi (Fig. 6c).

3 Miniaturized MTS antennas

To obtain a bandwidth of 30% with a dielectric constant of 3.55, the aforementioned open-ended MTS antennas usually have a finite MTS of $0.7\lambda_0 \times 0.7\lambda_0 \times 0.06\lambda_0$, while the short-ended MTS antennas occupy a smaller MTS of $0.6\lambda_0 \times 0.6\lambda_0 \times 0.06\lambda_0$. With the rapid development of wireless systems, miniaturized wideband antennas have been increasingly demanded in the wide-scanning phased arrays and compact multiple antenna systems. Therefore, three illustrative examples of the aperture miniaturization of wideband low-profile MTS antennas are discussed. Fig. 7a shows the structures of two

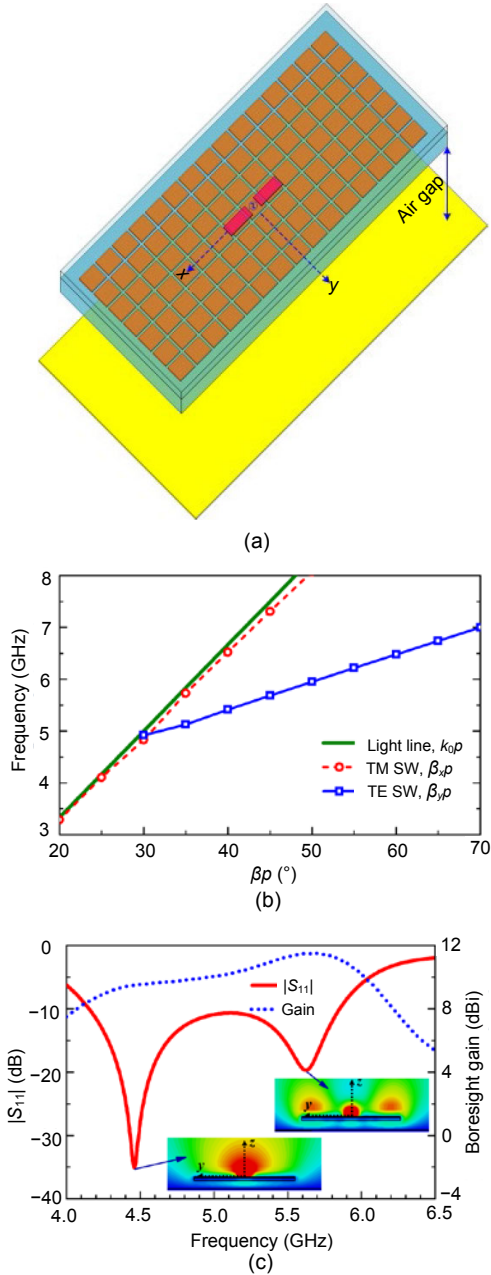


Fig. 6 SWR MTS antenna: (a) antenna structure; (b) surface wave dispersion diagram of the MTS unit; (c) simulated $|S_{11}|$ and realized boresight gain

aperture-coupled miniaturized MTS antennas with a reduced number of composed cells (Liu et al., 2017b). Ants *A* and *B* consist of 2×2 cells in square and H-shape, respectively. Ant *A* with a miniaturized MTS of $0.45\lambda_0 \times 0.45\lambda_0 \times 0.05\lambda_0$ (λ_0 is the free-space wavelength at the center frequency of 10.1 GHz) achieves a bandwidth of 18.5%. Using an H-shaped stepped impedance resonator (SIR) as an MTS unit

cell, a simulated bandwidth of 13% is obtained from ant *B* with a further miniaturized MTS of $0.40\lambda_0 \times 0.37\lambda_0 \times 0.05\lambda_0$ (Fig. 7b).

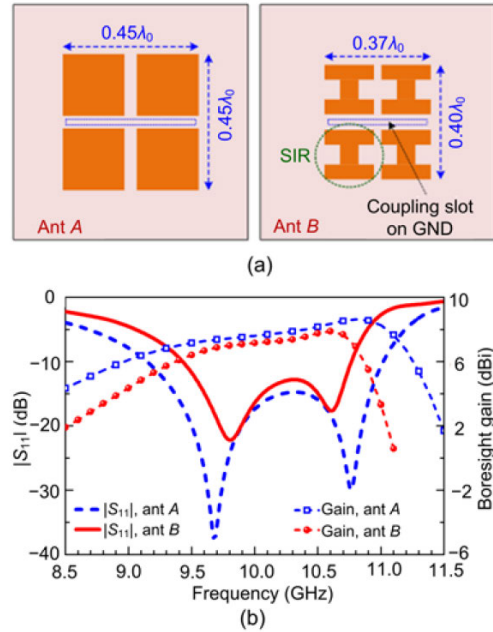


Fig. 7 Miniaturized MTS antennas: (a) antenna structures; (b) simulated $|S_{11}|$ and realized boresight gain

Another example of a miniaturized MTS antenna is shown in Fig. 8a, where a dual-layer overlapping MTS is constructed to increase the effective series capacitor C_L (Liu et al., 2017c). The dual-layer MTS provides much more freedom for the miniaturization antenna with achievable gap widths. As shown in Fig. 8a, a dual-layer MTS with a compact size of $0.43\lambda_0 \times 0.43\lambda_0 \times 0.06\lambda_0$ (λ_0 is the free-space wavelength at the center frequency of 5.5 GHz) achieves a bandwidth of 28%, realizing the gain ranging from 6.4 to 7.3 dBi and radiation efficiency of higher than 90%. Thus, increasing the capacitive coupling between the MTS cells represents a suitable miniaturization technique for wideband low-profile MTS antennas.

4 Multifunctional MTS antennas

To meet the increasing requirement for more functionalities, the dispersion-engineered wideband low-profile MTS antenna technique can be extended to realize circular polarization, filtering, enhanced

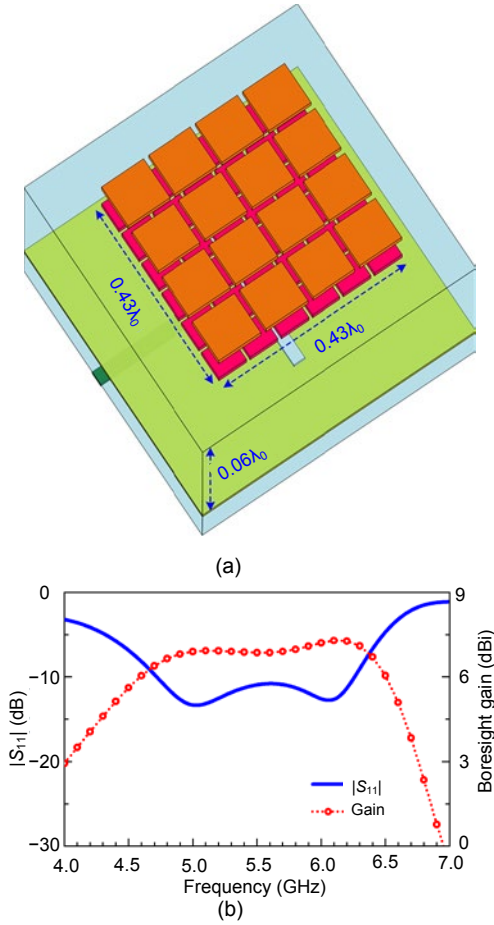


Fig. 8 Miniaturized dual-layer MTS antenna: (a) antenna structure; (b) simulated $|S_{11}|$ and realized boresight gain

beam-scanning capability, low RCS, dual wideband, and reconfigurability. Various antennas are reviewed in this section.

4.1 Circularly polarized antennas

The CP radiation is an important functionality and is desired in many applications because of its improved immunity to multipath distortion and polarization mismatch losses. The single-feed CP radiation can be generated by exciting two orthogonal modes with a 90° phase difference. Recent progress in the single-feed CP antenna design using the dispersion-engineered low-profile MTS is summarized with performance comparison (Fig. 9). The CP performance can be realized by Z-shaped slot coupling (Lin et al., 2015), L-shaped slot coupling (Chen et al., 2018), CP patch feed (Ta and Park, 2015), asymmetrical MTS (Huang et al., 2016; Zheng et al., 2018;

Juan et al., 2019), or combining asymmetrical MTS with the slant slot coupling or cross-slot coupling (Wu et al., 2016; Zhou et al., 2017; Zhao and Wang, 2018). Among these CP antennas, the MTS antenna proposed by Zhou et al. (2017) achieves the widest 3-dB axial ratio (AR) bandwidth of 44.4% with an MTS of $0.57\lambda_0 \times 0.31\lambda_0 \times 0.121\lambda_0$ (λ_0 is the free-space wavelength at the center frequency of 5.025 GHz). The cross slot with distributed circuit elements generates two electric fields with a 90° phase difference for the primary CP radiation. The asymmetrical MTS is designed to further widen the AR bandwidth. The CP MTS antenna proposed by Juan et al. (2019) has the most compact design. By introducing a pair of capacitive-loading strips along the diagonal of a corner-truncated MTS unit cell, the size of the CP MTS has been reduced to $0.56\lambda_0 \times 0.56\lambda_0 \times 0.037\lambda_0$ (λ_0 is the free-space wavelength at the center frequency of 3.45 GHz), and its 3-dB AR bandwidth is 8.7%.

4.2 Enhanced-scanning phased arrays

The wideband wide-angle beam scanning phased arrays are highly desired in a wide range of applications, such as radar and satellite communication systems. The potential use of MTS for wide-angle beam scanning is demonstrated by an illustrative example in Fig. 10a (Li M et al., 2015). The surface wave dispersion of the MTS is engineered to ensure the TE SW to propagate within the operating band of the phase array, contributing to the wide beamwidth of individual antenna elements and wide-angle scanning performance of the phased array. With a uniform amplitude and progressive phase excitation, the low-profile MTS-based array exhibits a wide scanning angle of up to 85° in the H-plane. The gain fluctuation is less than 3 dB, and sidelobe levels are lower than -10 dB in the whole scanning range. As shown in Fig. 10b, the aperture-coupled low-profile RH MTS antenna can be employed to realize a wideband wide-range scanning phased array with the MTS-radiator sharing approach and defected ground structures (DGS) (Gu et al., 2017). The MTS antenna array with a low profile of $0.049\lambda_0$ (λ_0 is the free-space wavelength at the center frequency of 5.2 GHz) can achieve a bandwidth of 23% and a maximum scanning angle of 50° in the H-plane. Fig. 10c shows an MTS-based CP phased array for Ka-band applications, where a dual-layer overlapping

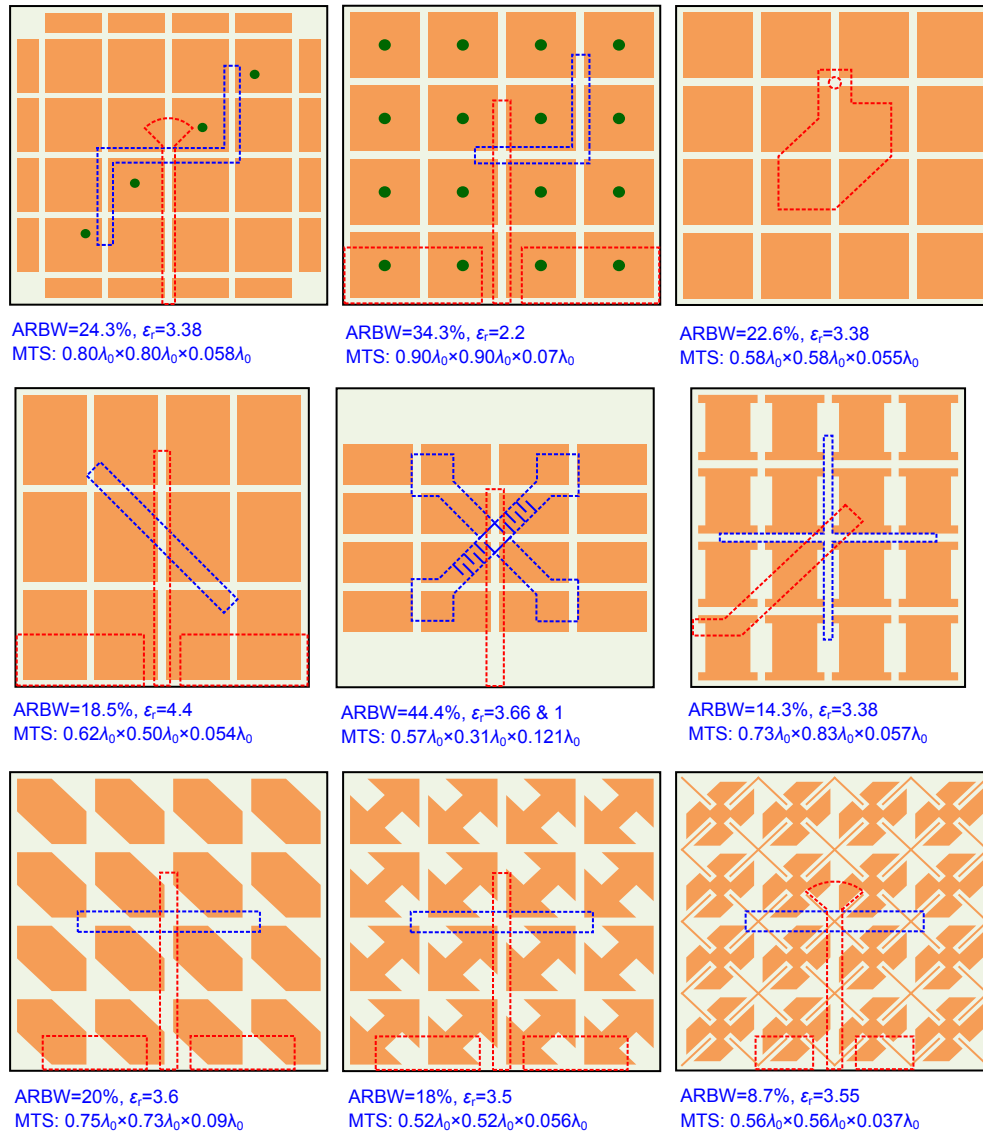


Fig. 9 Circularly polarized metasurface antennas with comparison of performances and dimensions

MTS is used for antenna miniaturization and a cross slot coupled by a single series stripline feed is designed for CP generation (Liu et al., 2017a). The 64-element MTS phased array can achieve a 2D beam scanning with a maximum scan angle of 30° off the boresight direction over the frequency range of 28–31 GHz.

4.3 Other antennas

Considering both the particular reflection properties in the normal direction and the dispersion properties of the guided waves in the transverse direction, the MTSs can be engineered to realize both wideband broadside radiation and wideband RCS

reduction. By replacing the surrounding metallic ground plane with a bandstop frequency selective surface, a wideband low-RCS high-gain mushroom-like antenna can be realized (Jia et al., 2015). The chessboard configuration of asymmetrical MTSs enables the antiphase reflection under the orthogonally polarized incident waves for scattering. Accordingly, the sequentially fed MTS antenna arrays can be designed for wideband CP radiation with a low RCS (Zhao et al., 2017; Zhang et al., 2019).

The non-uniform MTS can be used to realize a wideband filtering antenna in wireless systems for miniaturizing circuit size and enhancing overall performance (Pan et al., 2016). An MTS-based

shared-aperture antenna has been proposed for incoming 5G dual-band applications (Li and Chen, 2018). Recently, a wideband low-profile MTS antenna has been employed to realize the high-performance steerable dual-beam using a novel symmetrical controllable feeding network (Yang et al., 2019) and to achieve the reconfigurable polarization using a simple DC controlling circuit (Wu et al., 2019).

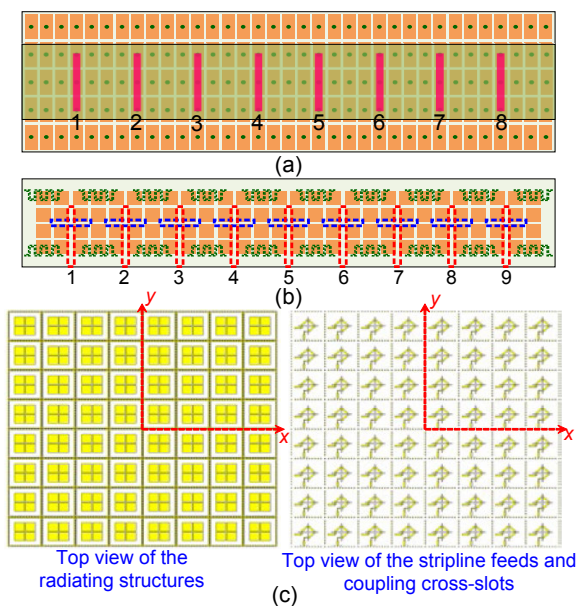


Fig. 10 MTS-based phased array with surface wave excitation (a), phased array with shared MTS radiators and defected ground structures (b), and MTS-based circularly polarized phased array (c)

5 Conclusions

The historical and recent development of the dispersion-engineered wideband low-profile MTS antenna technology has been reviewed in detail. The operation of an MTS antenna depends on the dispersion relation of guided/surface waves, specified boundary conditions, and feeding methods. The successful development of MTS antennas has clearly demonstrated that owing to the great freedom to control the radiation characteristics, the dispersion-engineered MTS antenna technology is promising for innovative antenna design. More exciting achievements and industrial applications of the MTS antenna technology can be expected in the near future.

Contributors

Wei E. I. LIU contributed to the idea, simulation, theoretical analysis, and measurement. Zhi Ning CHEN and Xianming QING contributed to the idea, technical discussion, and measurement. Wei E. I. LIU wrote the manuscript. All the authors reviewed the manuscript.

Compliance with ethics guidelines

Wei E. I. LIU, Zhi Ning CHEN, and Xianming QING declare that they have no conflict of interest.

References

- Caloz C, Itoh T, 2005. *Electromagnetic Metamaterials: Transmission Line Theory and Microwave Applications*. Wiley-IEEE Press, New York, USA.
<https://doi.org/10.1002/0471754323>
- Chen DX, Yang WC, Che WQ, et al., 2019. Broadband stable-gain multiresonance antenna using nonperiodic square-ring metasurface. *IEEE Antenn Wirel Propag Lett*, 18(8): 1537-1541. <https://doi.org/10.1109/LAWP.2019.2919692>
- Chen HT, Taylor AJ, Yu NF, 2016. A review of metasurfaces: physics and applications. *Rep Prog Phys*, 79(7):076401. <https://doi.org/10.1088/0034-4885/79/7/076401>
- Chen Q, Zhang H, Shao YJ, et al., 2018. Bandwidth and gain improvement of an L-shaped slot antenna with metamaterial loading. *IEEE Antenn Wirel Propag Lett*, 17(8): 1411-1415. <https://doi.org/10.1109/LAWP.2018.2848639>
- Costa F, Luukkonen O, Simovski CR, et al., 2011. TE surface wave resonances on high-impedance surface based antennas: analysis and modeling. *IEEE Trans Antenn Propag*, 59(10):3588-3596. <https://doi.org/10.1109/TAP.2011.2163750>
- Eleftheriades GV, Balmain KG, 2005. *Negative-Refractive Metamaterials: Fundamental Principles and Applications*. Wiley-IEEE Press, New York, USA.
<https://doi.org/10.1002/0471744751>
- Erfani E, Niroo-Jazi M, Tatu S, 2016. A high-gain broadband gradient refractive index metasurface lens antenna. *IEEE Trans Antenn Propag*, 64(5):1968-1973. <https://doi.org/10.1109/TAP.2016.2526052>
- Glybovski SB, Tretyakov SA, Belov PA, et al., 2016. Metasurfaces: from microwaves to visible. *Phys Rep*, 634:1-72. <https://doi.org/10.1016/j.physrep.2016.04.004>
- Gu L, Zhao YW, Cai QM, et al., 2017. Scanning enhanced low-profile broadband phased array with radiator-sharing approach and defected ground structures. *IEEE Trans Antenn Propag*, 65(11):5846-5854. <https://doi.org/10.1109/TAP.2017.2754321>
- Holloway CL, Kuester EF, Gordon JA, et al., 2012. An overview of the theory and applications of metasurfaces: the two-dimensional equivalents of metamaterials. *IEEE Antenn Propag Mag*, 54(2):10-35. <https://doi.org/10.1109/MAP.2012.6230714>
- Huang YJ, Yang L, Li J, et al., 2016. Polarization conversion of metasurface for the application of wide band low-profile circular polarization slot antenna. *Appl Phys Lett*, 109(5):

054101. <https://doi.org/10.1063/1.4960198>
- Jia YT, Liu Y, Wang H, et al., 2015. Low-RCS, high-gain, and wideband mushroom antenna. *IEEE Antenn Wirel Propag Lett*, 14:277-280. <https://doi.org/10.1109/LAWP.2014.2363071>
- Jiang M, Chen ZN, Zhang Y, et al., 2017. Metamaterial-based thin planar lens antenna for spatial beamforming and multibeam massive MIMO. *IEEE Trans Antenn Propag*, 65(2):464-472. <https://doi.org/10.1109/TAP.2016.2631589>
- Juan Y, Yang WC, Che WQ, 2019. Miniaturized low-profile circularly polarized metasurface antenna using capacitive loading. *IEEE Trans Antenn Propag*, 67(5):3527-3532. <https://doi.org/10.1109/TAP.2019.2902735>
- Li AB, Singh S, Sievenpiper D, 2018. Metasurfaces and their applications. *Nanophotonics*, 7(6):989-1011. <https://doi.org/10.1515/nanoph-2017-0120>
- Li HP, Wang GM, Xu HX, et al., 2015. X-band phase-gradient metasurface for high-gain lens antenna application. *IEEE Trans Antenn Propag*, 63(11):5144-5149. <https://doi.org/10.1109/TAP.2015.2475628>
- Li M, Xiao SQ, Wang BZ, 2015. Investigation of using high impedance surfaces for wide-angle scanning arrays. *IEEE Trans Antenn Propag*, 63(7):2895-2901. <https://doi.org/10.1109/TAP.2015.2421936>
- Li T, Chen ZN, 2018. Metasurface-based shared-aperture 5G S-/K-band antenna using characteristic mode analysis. *IEEE Trans Antenn Propag*, 66(12):6742-6750. <https://doi.org/10.1109/TAP.2018.2869220>
- Lin FH, Chen ZN, Liu W, et al., 2015. A metamaterial-based broadband circularly polarized aperture-fed grid-slotted patch antenna. IEEE 4th Asia-Pacific Conf on Antennas and Propagation, p.353-354. <https://doi.org/10.1109/APCAP.2015.7374401>
- Liu W, Chen ZN, Qing X, 2014a. Metamaterial-based low-profile broadband mushroom antenna. *IEEE Trans Antenn Propag*, 62(3):1165-1172. <https://doi.org/10.1109/TAP.2013.2293788>
- Liu W, Chen ZN, Qing X, 2014b. Stripline aperture coupled metamaterial mushroom antenna with increased front-to-back ratio. IEEE Antennas and Propagation Society Int Symp, p.444-445. <https://doi.org/10.1109/APS.2014.6904554>
- Liu W, Chen ZN, Qing X, 2014c. 60-GHz thin broadband high-gain LTCC metamaterial—mushroom antenna array. *IEEE Trans Antenn Propag*, 62(9):4592-4601. <https://doi.org/10.1109/TAP.2014.2333052>
- Liu W, Chen ZN, Qing X, 2015a. Metamaterial-based low-profile broadband aperture-coupled grid-slotted patch antenna. *IEEE Trans Antenn Propag*, 63(7):3325-3329. <https://doi.org/10.1109/TAP.2015.2429741>
- Liu W, Qing X, Chen ZN, 2015b. Metamaterial-based wideband shorting-wall loaded mushroom array antenna. 9th European Conf on Antennas and Propagation, p.1-4.
- Liu WEI, Chen ZN, Qing X, 2017a. Compact wideband metasurface-based circularly polarized antenna for Ka-band phased array. IEEE-APS Tropical Conf on Antennas and Propagation in Wireless Communications, p.17-21. <https://doi.org/10.1109/APWC.2017.8062229>
- Liu W, Chen ZN, Qing X, 2017b. Miniaturized broadband metasurface antenna using stepped impedance resonators. IEEE 5th Asia-Pacific Conf on Antennas and Propagation, p.365-366. <https://doi.org/10.1109/APCAP.2016.7843245>
- Liu WEI, Chen ZN, Qing X, et al., 2017c. Miniaturized wideband metasurface antennas. *IEEE Trans Antenn Propag*, 65(12):7345-7349. <https://doi.org/10.1109/TAP.2017.2761550>
- Liu W, Chen ZN, Qing X, 2017d. Mode analysis and experimental verification of shorting-wall loaded mushroom antenna. Asia-Pacific Microwave Conf, p.1-4. <https://doi.org/10.1109/APMC.2016.7931342>
- Luukkonen O, Simovski C, Granet G, et al., 2008. Simple and accurate analytical model of planar grids and high-impedance surfaces comprising metal strips or patches. *IEEE Trans Antenn Propag*, 56(6):1624-1632. <https://doi.org/10.1109/TAP.2008.923327>
- Pan YM, Hu P, Zhang XY, et al., 2016. A low-profile high-gain and wideband filtering antenna with metasurface. *IEEE Trans Antenn Propag*, 64(5):2010-2016. <https://doi.org/10.1109/TAP.2016.2535498>
- Shelby RA, Smith DR, Schultz S, 2001. Experimental verification of a negative index of refraction. *Science*, 292(5514):77-79. <https://doi.org/10.1126/science.1058847>
- Sievenpiper D, Zhang LJ, Broas RFJ, et al., 1999. High-impedance electromagnetic surfaces with a forbidden frequency band. *IEEE Trans Microw Theor Techn*, 47(11):2059-2074. <https://doi.org/10.1109/22.798001>
- Smith DR, Padilla WJ, Vier DC, et al., 2000. Composite medium with simultaneously negative permeability and permittivity. *Phys Rev Lett*, 84(18):4184-4187. <https://doi.org/10.1103/PhysRevLett.84.4184>
- Sun WY, Li Y, Zhang ZJ, et al., 2019. Low-profile and wideband microstrip antenna using quasi-periodic aperture and slot-to-CPW transition. *IEEE Trans Antenn Propag*, 67(1):632-637. <https://doi.org/10.1109/TAP.2018.2874801>
- Syed Nasser SS, Liu W, Chen ZN, 2018. Wide bandwidth and enhanced gain of a low-profile dipole antenna achieved by integrated suspended metasurface. *IEEE Trans Antenn Propag*, 66(3):1540-1544.
- Ta SX, Park I, 2015. Low-profile broadband circularly polarized patch antenna using metasurface. *IEEE Trans Antenn Propag*, 63(12):5929-5934. <https://doi.org/10.1109/TAP.2015.2487993>
- Wang JF, Wong H, Ji ZQ, et al., 2019. Broadband CPW-fed aperture coupled metasurface antenna. *IEEE Antenn Wirel Propag Lett*, 18(3):517-520. <https://doi.org/10.1109/LAWP.2019.2895618>
- Wu Z, Li L, Li YJ, et al., 2016. Metasurface superstrate

- antenna with wideband circular polarization for satellite communication application. *IEEE Antenn Wirel Propag Lett*, 15:374-377.
<https://doi.org/10.1109/LAWP.2015.2446505>
- Wu Z, Liu HX, Li L, 2019. Metasurface-inspired low profile polarization reconfigurable antenna with simple DC controlling circuit. *IEEE Access*, 7:45073-45079.
<https://doi.org/10.1109/ACCESS.2019.2908928>
- Yang F, Rahmat-Samii Y, 2003. Microstrip antennas integrated with electromagnetic band-gap (EBG) structures: a low mutual coupling design for array applications. *IEEE Trans Antenn Propag*, 51(10):2936-2946.
<https://doi.org/10.1109/TAP.2003.817983>
- Yang WC, Chen S, Che WQ, et al., 2018. Compact high-gain metasurface antenna arrays based on higher-mode SIW cavities. *IEEE Trans Antenn Propag*, 66(9):4918-4923.
<https://doi.org/10.1109/TAP.2018.2851659>
- Yang WC, Gu LZ, Che WQ, et al., 2019. A novel steerable dual-beam metasurface antenna based on controllable feeding mechanism. *IEEE Trans Antenn Propag*, 67(2):784-793. <https://doi.org/10.1109/TAP.2018.2880089>
- Zhang WB, Liu Y, Jia YT, 2019. Circularly polarized antenna array with low RCS using metasurface-inspired antenna units. *IEEE Antenn Wirel Propag Lett*, 18(7):1453-1457.
<https://doi.org/10.1109/LAWP.2019.2919716>
- Zhao C, Wang CF, 2018. Characteristic mode design of wide band circularly polarized patch antenna consisting of H-shaped unit cells. *IEEE Access*, 6:25292-25299.
<https://doi.org/10.1109/ACCESS.2018.2828878>
- Zhao Y, Cao XY, Gao J, et al., 2017. Broadband low-RCS circularly polarized array using metasurface-based element. *IEEE Antenn Wirel Propag Lett*, 16:1836-1839.
<https://doi.org/10.1109/LAWP.2017.2682848>
- Zheng Q, Guo CJ, Ding J, 2018. Wideband and low RCS circularly polarized slot antenna based on polarization conversion of metasurface for satellite communication application. *Microw Opt Technol Lett*, 60(3):679-685.
<https://doi.org/10.1002/MOP.31026>
- Zhou CF, Cheung SW, Li QL, et al., 2017. Bandwidth and gain improvement of a crossed slot antenna with metasurface. *Appl Phys Lett*, 110(21):211603.
<https://doi.org/10.1063/1.4984276>